

An Efficient Technique to Determine the Power Spectrum from Cosmic Microwave Background Sky Maps

Siang Peng Oh, David N. Spergel
Princeton University Observatory, NJ 08544

and

Gary Hinshaw
Goddard Flight Space Center, MD 20771

ABSTRACT

There is enormous potential to advance cosmology from statistical characterizations of cosmic microwave background sky maps. The angular power spectrum of the microwave anisotropy is a particularly important statistic. Existing algorithms for computing the angular power spectrum of a pixelized map typically require $O(N^3)$ operations and $O(N^2)$ storage, where N is the number of independent pixels in the map. The *MAP* and *Planck* satellites will produce megapixel maps of the cosmic microwave background temperature at multiple frequencies; thus, existing algorithms are not computationally feasible. In this article, we introduce an algorithm that requires $O(N^2)$ operations and $O(N^{3/2})$ storage that can find the minimum variance power spectrum from sky map data roughly one million times faster than was previously possible. This makes feasible an analysis that was hitherto intractable.

1. Introduction

The *MAP* and *Planck* satellites have the potential to yield enormous amounts of information about the physical conditions in the early universe (Bennett et al. 1995; <http://map.gsfc.nasa.gov>; Bersanelli et al. 1996; <http://astro.estec.esa.nl/Planck>). For example, with full sky coverage and an angular resolution of 0.21° at its highest frequency, *MAP* should return accurate measurements of the cosmic microwave background (CMB) temperature anisotropy at roughly one million independent points on the sky. If the temperature fluctuations are consistent with inflationary models, these measurements will provide accurate determinations of most of the significant cosmological parameters (Spergel 1994; Knox 1995; Hinshaw, Bennett & Kogut 1995; Jungman et al. 1996; Zaldarriaga, Spergel & Seljak 1997; Bond, Efstathiou & Tegmark 1997). If they are not consistent with

inflationary models, it will be even more exciting as we will need to rethink our ideas about the physics of the early universe.

There are a number of non-trivial numerical steps involved in comparing 10^{11} temperature differences with the predictions of a particular cosmological model. Several of the steps in the calculation are now clear. Wright, Hinshaw & Bennett (1996) found a rapid and exact algorithm for producing megapixel cosmic microwave background maps from differential data. Seljak & Zaldarriaga (1996) present a fast algorithm for computing the power spectrum for a given cosmological model. However, to date, we have lacked an efficient technique for computing the power spectrum from an observed sky map. The techniques that were used to extract the power spectrum from the *COBE* data (Górski 1994; Górski et al. 1994; Bond 1995; Tegmark & Bunn 1995; Górski et al. 1996; Hinshaw et al. 1996; Tegmark 1996) cannot easily be extended to the high resolution data since these techniques require $O(N^3)$ operations and $O(N^2)$ storage. For a single frequency of *MAP* data, for example, this would take $> 10^{19}$ operations, with $> 10^{21}$ operations required for a combined analysis of polarization and temperature maps.

In this paper, we present a fast, accurate method for extracting the power spectrum from realistic simulations of high resolution data at a single frequency. In §2-5 we develop our numerical method for determining the power spectrum from data containing only cosmological signal and detector noise. In §6, we show how the same approach can be used to directly estimate cosmological parameters from the maps. In §7, we apply the method to realistic simulations of *MAP* data that include spatially varying noise and a galactic sky cut. We show that our numerical method recovers minimum variance, unbiased estimates of the power spectrum and of cosmological parameters. We summarize our results in §8. A subsequent paper will extend the techniques developed here to the analysis of multi-frequency data and polarization data.

2. Maximum Likelihood Determination of the Power Spectrum

The basic problem is to extract the angular power spectrum of the CMB temperature fluctuations from noisy data. We can expand the CMB temperature in spherical harmonics,

$$\delta t(\Omega) = \sum_{l,m} a_{lm}^{sky} w_l Y_{lm}(\Omega) \quad (1)$$

where w_l is Legendre expansion of the experimental window function. If inflationary models are correct, the a_{lm}^{sky} coefficients are uncorrelated Gaussian random variables with zero mean

and a variance that is independent of orientation

$$\langle a_{lm}^{sky} a_{l'm'}^{sky*} \rangle = c_l^{sky} \delta_{ll'} \delta_{mm'} \quad (2)$$

where c_l^{sky} is the angular power spectrum we wish to estimate from the maps.

Like *COBE*, *MAP* and *Planck* will produce full sky maps at a number of frequencies. In this paper, we will focus on the analysis of the highest resolution map from *MAP* (0.21° at 94 GHz), which is expected to contain useful signal up to at least multipole order $l \sim 1000$. The data in a given map may be expressed as a superposition of several terms

$$\mathbf{m} = \delta\mathbf{t} + \mathbf{n} + \mathbf{g} + \mathbf{f} \quad (3)$$

where $\delta\mathbf{t}$ is the CMB signal convolved with the instrument's beam response, \mathbf{n} is the detector noise, \mathbf{g} is the systematic error, and \mathbf{f} is the foreground emission. Note that the measurement vector \mathbf{m} can be expressed either in a pixel basis, with components m_i , the observed temperature in pixel i , or in a spherical harmonic basis, with components $m_{lm} = a_{lm}$, the observed moment of the spherical harmonic Y_{lm} . The choice of basis to use for power spectrum estimation requires weighing many trade-offs which we discuss in this and subsequent sections. Key among these is the form of the covariance matrix that describes the data, \mathbf{m} .

While *MAP* will measure temperature fluctuations across the entire sky, we will want to exclude pixels in the Galactic plane from our analysis, as well as other randomly located pixels that contain bright, non-cosmological sources. In this paper, we will assume that we can remove foreground emission by simply excluding the galactic plane and bright sources. The resulting incomplete coverage of the celestial sphere precludes naively evaluating a spherical harmonic expansion of the data by direct integration. The analysis is further complicated by *MAP*'s inhomogeneous sampling of the sky: the noise per unit area will vary by more than a factor two between the ecliptic poles and the equator. *MAP*'s differential design has been optimized to minimize systematic errors and to produce maps with spatially uncorrelated noise. We will assume that we can ignore systematic errors and that the noise is uncorrelated from pixel to pixel. We have not yet tested the performance of our algorithm with maps that contain significant pixel to pixel noise correlations or “stripes”.

With the above assumptions, the covariance matrix of the data takes the form $\mathbf{C} \equiv \langle \mathbf{m}\mathbf{m}^T \rangle = \mathbf{S} + \mathbf{N}$ where $\mathbf{S} = \langle \delta\mathbf{t}\delta\mathbf{t}^T \rangle$ is the covariance of the CMB fluctuations, and $\mathbf{N} = \langle \mathbf{n}\mathbf{n}^T \rangle$ is the covariance matrix of the noise. In the pixel basis, the noise matrix is diagonal ($\mathbf{N}_{ij} = \sigma_i^2 \delta_{ij}$, where σ_i is the *rms* noise in pixel i) while in the spherical harmonic basis the signal matrix is diagonal

$$\mathbf{S}_{(lm)(lm')} \equiv \langle a_{lm}^{sky} a_{l'm'}^{sky*} \rangle w_l w_{l'} = c_l^{sky} w_l^2 \delta_{(lm)(lm')}. \quad (4)$$

For the sake of notational simplicity, we shall henceforth set

$$c_l = c_l^{sky} w_l^2 \quad (5)$$

and solve for c_l . Note that the signal matrix in the pixel basis can be easily expressed in terms of spherical harmonics

$$\mathbf{S}_{ij} \equiv \langle \delta t_i \delta t_j \rangle = \sum_{(lm), (lm)'} Y_{lm}(\Omega_i) \mathbf{S}_{(lm)(lm)'} Y_{l'm'}^*(\Omega_j) \equiv \mathbf{Y} \mathbf{S} \mathbf{Y}^* \quad (6)$$

where \mathbf{Y}^* is the complex conjugate of \mathbf{Y} . The form of the noise matrix in the spherical harmonic basis is deferred to the next section.

We wish to estimate the angular power spectrum from the data by explicitly maximizing the likelihood function, which, for Gaussian fluctuations, has the form

$$\mathcal{L}(c_l | \mathbf{m}) = \frac{\exp\left(-\frac{1}{2} \mathbf{m}^T \mathbf{C}^{-1} \mathbf{m}\right)}{(2\pi)^{N/2} (\det \mathbf{C})^{1/2}} \quad (7)$$

where \mathbf{C} is the full covariance matrix. A number of authors (Górski 1994; Górski et al. 1994; Bond 1995; Tegmark & Bunn 1995; Górski et al. 1996; Hinshaw et al. 1996; Tegmark 1996) have used this approach to extract the power spectrum from the *COBE* data.

We find the most likely power spectrum by expanding the likelihood function as a Taylor series

$$f \equiv -2 \ln \mathcal{L} = \bar{f} + \sum_l \left. \frac{\partial f}{\partial c_l} \right|_{\bar{c}_l} (c_l - \bar{c}_l) + \sum_{l,l'} \frac{1}{2} \left. \frac{\partial^2 f}{\partial c_l \partial c_{l'}} \right|_{\bar{c}_l} (c_l - \bar{c}_l) (c_{l'} - \bar{c}_{l'}) \quad (8)$$

where the over-bar indicates the values at which f is minimized. Differentiating equation (7) yields

$$\frac{\partial f}{\partial c_l} = - \left(\frac{\partial}{\partial c_l} \right) 2 \ln \mathcal{L} = - \mathbf{m}^T \mathbf{C}^{-1} \mathbf{P}^l \mathbf{C}^{-1} \mathbf{m} + \text{tr}(\mathbf{C}^{-1} \mathbf{P}^l) \quad (9)$$

where

$$\mathbf{P}^l \equiv \frac{\partial \mathbf{C}}{\partial c_l}. \quad (10)$$

In the spherical harmonic basis \mathbf{P}^l is a diagonal matrix with entries 0 or 1, while in the pixel basis, it is given by

$$\mathbf{P}_{ij}^l = \frac{(2l+1)}{4\pi} P_l(\cos \gamma_{ij}) \quad (11)$$

where P_l is the Legendre polynomial of order l , and γ_{ij} is the angle between pixels i and j . The second order term in the likelihood function is

$$\frac{1}{2} \frac{\partial^2 f}{\partial c_l \partial c_{l'}} = \mathbf{m}^T \mathbf{C}^{-1} \mathbf{P}^l \mathbf{C}^{-1} \mathbf{P}^{l'} \mathbf{C}^{-1} \mathbf{m} - \frac{1}{2} \text{tr}(\mathbf{C}^{-1} \mathbf{P}^l \mathbf{C}^{-1} \mathbf{P}^{l'}). \quad (12)$$

The expectation value of this quantity is the Fisher matrix

$$\mathbf{F}_{ll'} = \left\langle - \left(\frac{\partial^2}{\partial c_l \partial c_{l'}} \right) \ln \mathcal{L} \right\rangle = \frac{1}{2} \text{tr}(\mathbf{C}^{-1} \mathbf{P}^l \mathbf{C}^{-1} \mathbf{P}^{l'}) \quad (13)$$

where we have used $\langle \mathbf{m} \mathbf{m}^T \rangle = \mathbf{C}$.

We can locate the most-likely power spectrum by finding where the derivative of the likelihood function is zero. Let $c_l^{(0)}$ be a trial power spectrum, then the derivative of the likelihood in the neighborhood of $c_l^{(0)}$ may be written

$$\left. \frac{\partial f}{\partial c_l} \right|_{c_l} \simeq \left. \frac{\partial f}{\partial c_l} \right|_{c_l^{(0)}} + 2 \sum_{l'} \mathbf{F}_{ll'} (c_{l'} - c_{l'}^{(0)}) = 0 \quad (14)$$

where we have approximated the second derivative by its expectation value. This suggests solving for the most-likely power spectrum using a variable metric method,

$$c_l^{(n+1)} = c_l^{(n)} - \frac{1}{2} \sum_{l'} \mathbf{F}_{ll'}^{-1} \left. \frac{\partial f}{\partial c_{l'}} \right|_{c_{l'}^{(n)}}. \quad (15)$$

Note that this is exactly the Newton-Raphson method for non-linear systems of equations (Press et al. 1992), which is well known to converge quadratically near the neighborhood of a root. Its only potential problem is its poor global convergence properties, which can occur when the approximation in equation (8) is not valid. In practice, we have found the likelihood function is sufficiently well-behaved that this is never a problem, even with extremely poor starting guesses. The structureless nature of the likelihood function has also been noted by other authors (Bond, Jaffe & Knox 1998). This is easy to understand intuitively. As we demonstrate later the c_l parameters are only weakly correlated with each other as the Fisher matrix is diagonally dominant. Thus, to first order, we are performing a series of one-parameter likelihood maximizations, with small corrections for couplings. In each dimension, the likelihood is very well approximated by a parabola (since the probability distribution for each c_l is close to Gaussian). In particular, no local extrema exist, so there is no danger in employing Newton-Raphson. This also explains the extremely rapid convergence of the method – typically 3-4 iterations.

Our equations are essentially equivalent to that of Tegmark (1997) and Bond, Jaffe & Knox (1998); however, we have recast them into a form that is computationally more tractable. The key advance is in reducing all ostensibly $O(N^3)$ operations to $O(N^2)$ operations. We highlight the crucial elements of this improvement below, and discuss them more fully in subsequent sections.

- $\mathbf{C}^{-1} \mathbf{m}$ – Rather than evaluating this expression directly using Choleski techniques, we solve it iteratively using conjugate gradient techniques (Press et al. 1992, Barrett et

al. 1994), which are applicable to symmetric, positive definite linear systems. A good approximate inverse or preconditioner, $\tilde{\mathbf{C}}^{-1}$, is essential to reducing the number of iterations required. We find such a preconditioner by exploiting the approximate azimuthal symmetry of the noise pattern on the sky. This approach requires $O((N/20)^{3/2})$ memory for storage and takes $O((N/20)^2)$ operations to compute. In addition, each iteration of the conjugate gradient method involves performing a matrix multiplication of the form $\mathbf{C}\mathbf{z}$ where \mathbf{z} is a vector. We speed this up by writing \mathbf{C} as a convolution of diagonal matrices and spherical harmonic transforms. By employing fast spherical harmonic transforms (Muciaccia, Natoli & Vittorio 1998; Driscoll & Healey 1994), we are able to reduce the cost of the matrix multiplication from $O(N^2)$ to $O(N^{3/2})$.

- $\text{tr}(\mathbf{C}^{-1}\mathbf{P}^l)$ – We first compute this term approximately by assuming azimuthal symmetry of the noise. We then compute it exactly using Monte Carlo simulations of maps and exploiting the fact that

$$\langle \mathbf{m}^T \mathbf{C}^{-1} \mathbf{P}^l \mathbf{C}^{-1} \mathbf{m} \rangle = \text{tr}(\mathbf{C}^{-1} \mathbf{P}^l) \quad (16)$$

where we have used $\langle \mathbf{m} \mathbf{m}^T \rangle = \mathbf{C}$. The errors obtained by computing the trace term with Monte Carlo simulations rather than exactly are $\sqrt{1 + 1/N_{mc}}$ times larger than the minimum variance errors, where N_{mc} is the number of simulations used to compute the trace. Thus, if we generate 100 simulations, our errors will be only 0.5% larger than the minimum variance errors. The total cost of this step is $O(N_{mc} N_{iter} N^{3/2})$, where N_{iter} is the number of iterations used to evaluate equation (15).

- \mathbf{F} – Note that we only require an approximate second derivative to converge to the maximum of the likelihood function – the solution is fully independent of \mathbf{F} . We therefore compute \mathbf{F} approximately using the preconditioner $\tilde{\mathbf{C}}^{-1}$ previously computed, which requires $O((N/20)^2)$ operations. Once we obtain the maximum likelihood c_l , we use Monte Carlo simulations to obtain their probability distribution and hence their errors.

3. Iterative Evaluation of the Term $\mathbf{C}^{-1}\mathbf{m}$

A key step in our analysis is to iteratively (and rapidly) solve the linear equation

$$\mathbf{C}\mathbf{z} = \mathbf{m} \quad (17)$$

using conjugate gradient techniques. Note that this solution is only used in the evaluation of terms of the form $\mathbf{m}^T \mathbf{C}^{-1} \mathbf{P}^l \mathbf{C}^{-1} \mathbf{m}$. Thus, we have complete freedom to obtain this solution in pixel space (where the data vector is simply the temperature map) or in spherical harmonic space (where the data vector is the least squares fit of spherical harmonic

coefficients to the temperature map). In pixel space, we can use the addition theorem for spherical harmonics to write

$$\mathbf{m}^T \mathbf{C}^{-1} \mathbf{P}^l \mathbf{C}^{-1} \mathbf{m} = \sum_{m=-l}^l \mathbf{m}^T \mathbf{C}^{-1} \mathbf{Y}_{lm}^* \mathbf{Y}_{lm} \mathbf{C}^{-1} \mathbf{m} \quad (18)$$

which involves taking spherical harmonic transforms of the filtered, cut map, $\mathbf{C}^{-1} \mathbf{m}$. In spherical harmonic space, \mathbf{P}^l is simply a diagonal matrix with ones or zeros along the diagonal, so the evaluation of $\mathbf{m}^T \mathbf{C}^{-1} \mathbf{P}^l \mathbf{C}^{-1} \mathbf{m}$ is even simpler.

Our choice of the appropriate space to work in is motivated by a second consideration: the conjugate gradient technique requires that we compute an appropriate preconditioner matrix. Given a linear system $\mathbf{A} \mathbf{x} = \mathbf{b}$, where \mathbf{A} is symmetric and positive definite, the preconditioner is a symmetric positive definite matrix $\widetilde{\mathbf{A}}$, such that $\widetilde{\mathbf{A}}^{-1} \mathbf{A} = \mathbf{I} + \mathbf{R}$, where the eigenvalues of \mathbf{R} are all less than 1. The preconditioned conjugate gradient technique then solves the system

$$\widetilde{\mathbf{A}}^{-1} \mathbf{A} \mathbf{x} = \widetilde{\mathbf{A}}^{-1} \mathbf{b} \quad (19)$$

by generating a series of search directions and improved iterates. Specifically, it generates a sequence of coupled recurrence relations for the residual vector $\mathbf{r}^{(i)} \equiv \mathbf{b} - \mathbf{A} \mathbf{x}^{(i)}$ and the search direction $\mathbf{p}^{(i)}$

$$\mathbf{r}^{(i)} = \mathbf{r}^{(i-1)} - \alpha_i \mathbf{A} \mathbf{p}^{(i)} \quad (20)$$

$$\mathbf{p}^{(i)} = \widetilde{\mathbf{A}}^{-1} \mathbf{r}^{(i-1)} + \beta_{i-1} \mathbf{p}^{(i-1)} \quad (21)$$

The scalar α_i is chosen to minimize the quadratic function $f(\mathbf{x}) = (\mathbf{x}^{(i)} - \hat{\mathbf{x}})^T \mathbf{A} (\mathbf{x}^{(i)} - \hat{\mathbf{x}})$, where $\hat{\mathbf{x}}$ is the exact solution to $\mathbf{A} \mathbf{x} = \mathbf{b}$

$$\alpha_i = \frac{\mathbf{r}^{(i-1)T} \widetilde{\mathbf{A}}^{-1} \mathbf{r}^{(i-1)}}{\mathbf{p}^{(i)T} \mathbf{A} \mathbf{p}^{(i)}}. \quad (22)$$

The scalar β_{i-1} is chosen to ensure that the residuals are $\widetilde{\mathbf{A}}^{-1}$ orthogonal (i.e., $\mathbf{r}^{(i)T} \widetilde{\mathbf{A}}^{-1} \mathbf{r}^{(j)} = 0$ for $i \neq j$)

$$\beta_{i-1} = \frac{\mathbf{r}^{(i-1)T} \widetilde{\mathbf{A}}^{-1} \mathbf{r}^{(i-1)}}{\mathbf{r}^{(i-2)T} \widetilde{\mathbf{A}}^{-1} \mathbf{r}^{(i-2)}}. \quad (23)$$

In this manner the quadratic function $f(\mathbf{x})$ of the improved iterate

$$\mathbf{x}^{(i)} = \mathbf{x}^{(i-1)} + \alpha_i \mathbf{p}^{(i)} \quad (24)$$

is minimized over the whole vector space of conjugate search directions already taken, $\{\mathbf{p}_1, \mathbf{p}_2, \dots\}$. The routine is initialized by setting $\mathbf{r}^{(0)} = \mathbf{b} - \mathbf{A} \mathbf{x}^{(0)}$ for some initial guess $\mathbf{x}^{(0)}$,

and setting $\mathbf{p}^{(1)} = \widetilde{\mathbf{A}}^{-1}\mathbf{x}^{(0)}$. In general, the number of search directions required to span the vector space of possible solutions is N ; the preconditioner reduces this by transforming the contours of $f(\mathbf{x})$ to be as spherical as possible. To the extent that this is achieved the number of independent directions to minimize over becomes very small and the conjugate gradient routine converges quadratically. More precisely, the number of iterations required is proportional to $\sqrt{\kappa_2}$, where κ_2 is the condition number of the matrix $\widetilde{\mathbf{A}}^{-1}\mathbf{A}$ (i.e., the ratio of its largest to smallest eigenvalue). Further details may be found in Barrett et al. (1994) and Press et al. (1992).

There are two conflicting requirements for a preconditioner: it must be a sufficiently good approximation to the true inverse that κ_2 is not too large, yet it must be sufficiently sparse that it is significantly easier to compute and store than the original matrix. From this comes our choice of the correct space to work in: at low l where the signal dominates, we want to work in spherical harmonic space (where \mathbf{S} is diagonal), while at high l , where the noise dominates, we want to work in pixel space (where \mathbf{N} is diagonal).

Thus, we begin by considering how to transform the system into spherical harmonic space. We can obtain the the best-fit multipole moments, $m_{lm} = w_l m_{lm}^{sky}$, by minimizing

$$\chi^2 = \sum_i \frac{1}{\sigma_i^2} \left[m_i - \sum_{l,m} m_{lm} Y_{lm}(\Omega_i) \right]^2 \quad (25)$$

where the sum is over the uncut pixels, σ_i is the *rms* noise in the i th pixel, m_i is the observed temperature of the i th pixel, Ω_i is the direction to the center of the i th pixel, and w_l is the Legendre transform of the experimental window function. By differentiating equation (25), we derive the normal equations (Press et al. 1992)

$$\mathbf{N}^{-1}\mathbf{m} = \mathbf{y} \quad (26)$$

where

$$\mathbf{N}_{(lm)(lm)'}^{-1} = \sum_i \frac{Y_{lm}(\Omega_i) Y_{l'm'}(\Omega_i)}{\sigma_i^2} \quad (27)$$

is the inverse of the noise matrix for the multipole moments, and

$$\mathbf{y}_{(lm)} = \sum_i \frac{m_i Y_{lm}(\Omega_i)}{\sigma_i^2} \quad (28)$$

is the variance weighted spherical harmonic transform of the temperature map. The solution of the set of normal equations is a minimum variance estimate of $\mathbf{m}_{(lm)}$ and the uncertainty in each multipole is determined by $\mathbf{N}_{(lm)(lm)'}$.

The normal equations are ill-conditioned because \mathbf{N}^{-1} has null vectors induced by the cut pixels. Fortunately, we do not need to compute \mathbf{m} , but rather $\mathbf{z} \equiv (\mathbf{S} + \mathbf{N})^{-1}\mathbf{m}$. We can do this by solving the linear system

$$(\mathbf{S} + \mathbf{N})\mathbf{z} = \mathbf{m} = \mathbf{N}\mathbf{y} \quad (29)$$

We can put this into a computationally more tractable form by multiplying both sides by $\mathbf{S}^{1/2}\mathbf{N}^{-1}$, giving

$$(\mathbf{I} + \mathbf{S}^{1/2}\mathbf{N}^{-1}\mathbf{S}^{1/2})\mathbf{S}^{1/2}\mathbf{z} = \mathbf{S}^{1/2}\mathbf{y} \quad (30)$$

The reason for putting the system in this form is twofold. First, it only involves \mathbf{N}^{-1} , not \mathbf{N} , which cannot be easily evaluated. Second, the matrix $\mathbf{A} \equiv \mathbf{I} + \mathbf{S}^{1/2}\mathbf{N}^{-1}\mathbf{S}^{1/2}$ (which we will apply the conjugate gradient technique to) is well conditioned in the sense that its eigenvalues only span a few orders of magnitude. The second term – which is explicitly the signal to noise ratio – is regularized by the presence of the identity matrix. Alternative forms such as $(\mathbf{N}^{-1} + \mathbf{S}^{-1})\mathbf{S}\mathbf{z} = \mathbf{y}$ do not share this property – these matrices have eigenvalues that span a wide dynamic range.

We obtain a good preconditioner by splitting the matrix into two parts

$$\widetilde{\mathbf{A}} = \begin{pmatrix} \mathbf{I} + \mathbf{S}^{1/2}\widetilde{\mathbf{N}}^{-1}\mathbf{S}^{1/2} & 0 \\ 0 & \mathbf{I} + \text{diag}(\mathbf{S}^{1/2}\widetilde{\mathbf{N}}^{-1}\mathbf{S}^{1/2}) \end{pmatrix} \quad (31)$$

where $\widetilde{\mathbf{N}}^{-1}$ is a sparse, approximate form of \mathbf{N}^{-1} , given below. The lower right hand block is used for large l where the noise dominates the signal, so that $\mathbf{S}^{1/2}\widetilde{\mathbf{N}}^{-1}\mathbf{S}^{1/2}$ is small. In this regime, we obtain $\mathbf{z} \approx \mathbf{y}$, the spherical harmonic transform of the inverse variance weighted map. At small l the signal dominates, so we need to be able to approximate the form of the full noise matrix. For *MAP* 2-year data, we find that the above preconditioner works well if we split the matrix at $l_{\text{cutoff}} = 512$.

We now make a brief detour to explore the structure of the inverse noise matrix by expanding it in terms of the Wigner 3- j symbols. This gives us both a computationally efficient method to evaluate \mathbf{N}^{-1} , and, more importantly, provides some insight into the structure of \mathbf{N}^{-1} due to the sky cut and noise pattern. We first expand the inverse variance (weight) map in spherical harmonics. The multipole moments of this map are

$$\mathbf{w}_{lm} = \sum_i \frac{Y_{lm}^*(\Omega_i)}{\sigma_i^2}. \quad (32)$$

Using the completeness of the spherical harmonics, we may expand the inverse noise matrix, equation (27), as

$$\mathbf{N}_{(lm)(lm)'}^{-1} = \sum_{(lm)''} \mathbf{w}_{(lm)''} \sum_i Y_{lm}(\Omega_i) Y_{l'm'}(\Omega_i) Y_{l''m''}(\Omega_i) \quad (33)$$

$$= \sum_{(lm)''} \mathbf{w}_{(lm)''} \left(\frac{(2l+1)(2l'+1)(2l''+1)}{4\pi} \right)^{1/2} \begin{pmatrix} l & l' & l'' \\ 0 & 0 & 0 \end{pmatrix} \begin{pmatrix} l & l' & l'' \\ m & m' & m'' \end{pmatrix}$$

where the terms in brackets are the 3- j symbols. The first symbol is only non-zero when $|l - l'| \leq l'' \leq |l + l'|$. The second symbol imposes the additional constraint that $m - m' + m'' = 0$. We use numerically stable recurrence relations (Schulten, Klaus & Gordon, 1975) to compute the symbols. Alternatively, \mathbf{N}^{-1} may be computed by direct summation, which also requires $O(N^{3/2})$ operations.

This expansion suggests a simple approximation to the weight matrix. The dominant feature in the weight map is the galactic sky cut which is, to first order, azimuthally symmetric in galactic coordinates. In the limit of pure azimuthal symmetry the weight matrix would be block diagonal (proportional to $\delta_{mm'}$). This suggests a preconditioner of the form

$$\widetilde{\mathbf{N}}_{(lm)(lm)'}^{-1} \equiv \mathbf{N}_{(lm)(lm)'}^{-1} \delta_{mm'}. \quad (34)$$

Since $(\mathbf{I} + \mathbf{S}^{1/2} \widetilde{\mathbf{N}}^{-1} \mathbf{S}^{1/2})$ is block diagonal, we can compute its inverse in $O(N^2)$ steps. It is actually significantly less than this, due to the decreasing size of the block matrices. The matrix $\widetilde{\mathbf{A}}^{-1}$ requires the largest amount of memory for storage, $O((N/20)^{3/2})$, where the savings in the prefactor result from the facts that 1) we only need the full matrix up to $l = 512$, 2) all of the block matrices are symmetric, 3) the blocks are of decreasing size as m increases, and 4) parity is preserved – the covariance between even and odd l terms vanishes. For a 2 million pixel map, only 100 MB of memory is required to store the preconditioner in double precision.

The block diagonal approximation is an excellent ansatz to which we need only apply small perturbative corrections. Why does it work so well? To answer this, we must understand the sparsity pattern of \mathbf{N}^{-1} or, equivalently, its diagnostic $\mathbf{w}_{(lm)}$. The *MAP* weight map is approximately axisymmetric in ecliptic coordinates. Rotation to galactic coordinates (which imposes a tilt of about 60°) introduces a smooth, azimuthal variation in the noise pattern that can be perturbatively expanded in a Fourier series $e^{im\phi}$. The approximation of galactic axisymmetry used in the preconditioner is the largest ($m = 0$) term in such an expansion. We can quantify the fall-off in $\mathbf{w}_{(lm)}$ with increasing m by computing the “power” at each m , defined as

$$c_m \equiv \frac{1}{(l_{max} + 1 - m)} \sum_{l=m}^{l_{max}} |\mathbf{w}_{lm}|^2. \quad (35)$$

Figure 1 shows that corrections to the $m = 0$ mode are at most a few percent. The only high frequency contribution to the weight map comes from point sources. Since they only occupy $\sim 5\%$ of the sky, their effect is small.

A note on overall computational cost: each iteration of the conjugate gradient routine requires forming the products $\mathbf{A}\mathbf{w}_1$ and $\widetilde{\mathbf{A}}^{-1}\mathbf{w}_2$ for some work vectors \mathbf{w}_1 and \mathbf{w}_2 . The former involves 2 products with diagonal matrices ($\mathbf{S}^{1/2}$) and a forward and inverse spherical harmonic transform, each $O(N^{3/2})$. The latter involves a matrix-vector multiplication where $\widetilde{\mathbf{A}}^{-1}$ has fewer than $O(N^{3/2})$ non-zero elements. Thus, the cost per iteration is $O(N^{3/2})$, and the total cost of solving the linear system is $O(N_{iter}N^{3/2})$. A good preconditioner is the key to minimizing N_{iter} – in its absence, $N_{iter} \sim N$. We find that the linear system, equation (29), can be solved in about 6 iterations for the specifications appropriate to the 2-year *MAP* data and the preconditioner specified above. This requires ~ 30 seconds to solve for a 500,000 pixel map, and ~ 250 seconds to solve for a 2 million pixel map, running as a single processor job on an SGI Origin 2000.

4. Computation of the Trace

While we can use the preconditioner to compute $\mathbf{m}^T\mathbf{C}^{-1}\mathbf{P}^l\mathbf{C}^{-1}\mathbf{m}$ rapidly, it is still very time consuming to evaluate $\text{tr}(\mathbf{C}^{-1}\mathbf{P}^l)$ for each value of l by iteratively solving a linear equation for each (lm) term in the trace. There are two approaches to avoiding a brute force evaluation of the full trace. 1) Approximate $\text{tr}(\mathbf{C}^{-1}\mathbf{P}^l)$ as $\text{tr}(\mathbf{S}^{-1/2}\widetilde{\mathbf{A}}^{-1}\mathbf{S}^{1/2}\widetilde{\mathbf{N}}^{-1}\mathbf{P}^l)$ using the fact that $\mathbf{C}^{-1} = \mathbf{S}^{-1/2}\mathbf{A}^{-1}\mathbf{S}^{1/2}\mathbf{N}^{-1}$. This returns a high quality estimate of c_l . 2) Evaluate the trace for a given c_l using Monte Carlo simulations of maps drawn from that spectrum. This approach exploits the fact that

$$\text{tr}(\mathbf{C}^{-1}\mathbf{P}^l) = \langle \mathbf{m}^T\mathbf{C}^{-1}\mathbf{P}^l\mathbf{C}^{-1}\mathbf{m} \rangle \quad (36)$$

where we have used $\langle \mathbf{m}\mathbf{m}^T \rangle = \mathbf{C}$. This is the most computationally expensive part of our algorithm: it requires $O(N_{mc}N_{iter}N^{3/2})$ operations. Therefore we first maximize the likelihood function using the approximate trace (method 1), only switching to the Monte Carlo evaluation of the trace once the former solution has converged. Since we are very close to the true answer at this point, the Monte Carlo solution converges very quickly. Note that the Monte Carlo method is guaranteed by construction to be unbiased. Additionally, we can include non-linear effects in the synthetic maps that are not easily modeled in the covariance matrix \mathbf{C} . This will both correctly alter the maximum likelihood point and propagate through to the error estimates. We can further generalize the method to incorporate all known effects in our analysis by simulating the full analysis pipeline, rather than just the processed map.

How many Monte Carlo evaluations of $\mathbf{q}^{(i)} \equiv \mathbf{m}^{(i)}\mathbf{C}^{-1}\mathbf{P}^l\mathbf{C}^{-1}\mathbf{m}^{(i)}$, where i is a realization index, are necessary to obtain an accurate determination of $\text{tr}(\mathbf{C}^{-1}\mathbf{P}^l)$? To

answer this question, we need to determine how the variance in $\mathbf{q}^{(i)}$ propagates through to variance in the recovered c_l . Suppose we were able to calculate $\langle \mathbf{q} \rangle$ exactly for a given power spectrum c_l (e.g., by using an infinite number of simulations). The variance in our recovered c_l would then be given by the Cramer-Rao minimum variance bound

$$\begin{aligned} \langle (\mathbf{c}^{\text{recovered}} - \mathbf{c}^{\text{true}})(\mathbf{c}^{\text{recovered}} - \mathbf{c}^{\text{true}})^T \rangle &= \frac{1}{4} \mathbf{F}^{-1} \langle (\mathbf{q} - \langle \mathbf{q} \rangle)(\mathbf{q} - \langle \mathbf{q} \rangle)^T \rangle \mathbf{F}^{-1} \\ &= \mathbf{F}^{-1} \end{aligned} \quad (37)$$

which implies

$$\langle (\mathbf{q} - \langle \mathbf{q} \rangle)(\mathbf{q} - \langle \mathbf{q} \rangle)^T \rangle = 4\mathbf{F} \quad (38)$$

Now we do not know $\langle \mathbf{q} \rangle$, but $\langle \mathbf{q} \rangle'$, obtained by averaging $\mathbf{q}^{(i)}$ over N_{mc} uncorrelated Monte Carlo simulations. Hence, $\langle \mathbf{q} \rangle'$ has a Gaussian distribution, with variance

$$\sigma_{\langle \mathbf{q} \rangle'}^2 = \frac{1}{N_{mc}} \sigma_{\mathbf{q}^{(i)}}^2 \quad (39)$$

which implies

$$\langle (\mathbf{c}^{\text{recovered}} - \mathbf{c}^{\text{true}})(\mathbf{c}^{\text{recovered}} - \mathbf{c}^{\text{true}})^T \rangle = \left(1 + \frac{1}{N_{mc}}\right) \mathbf{F}^{-1} \quad (40)$$

where we have added the errors in quadrature. Thus, if we average 100 Monte Carlos to evaluate $\langle \mathbf{q} \rangle'$, our errors will be only 0.5% larger than the minimum variance case.

We have verified these expectations numerically. For a 512×1024 pixel test map (note that this is smaller than the 1024×2048 map we analyze in subsequent sections), we recover c_l by maximizing the likelihood function, but in each instance we compute $\langle \mathbf{q} \rangle'$ using a different number of Monte Carlo simulations. For each solution $c_l^{(N_{mc})}$ we then compute

$$\chi_{N_{mc}}^2 = (\mathbf{c}^{(N_{mc})} - \mathbf{c}^{\text{true}})^T \mathbf{F} (\mathbf{c}^{(N_{mc})} - \mathbf{c}^{\text{true}}) \quad (41)$$

which is expected to have a mean of $(1 + 1/N_{mc})(l_{max} - 1)$. For consistency we must use the same Fisher matrix for each N_{mc} , but this only affects the overall normalization of $\chi_{N_{mc}}^2$. Here we have used the Fisher matrix of the true underlying power spectrum. Figure 2 shows that to a very good approximation

$$\left(\frac{\chi_{N_{mc}}^2}{l_{max} - 1} \right) \propto 1 + \frac{1}{N_{mc}}. \quad (42)$$

Note that the quadratic convergence of the Newton-Raphson method means that the number of significant digits is doubled at each iteration. We can match this rate of convergence by doubling the number of Monte Carlo simulations used to compute the trace at each iteration. This saves some computer time in the early iterations when high precision is not required.

5. The Fisher Matrix and Error Estimates

As with the trace, a good approximation to the true Fisher matrix is given by

$$\tilde{\mathbf{F}}_{ll'} = \frac{1}{2} \text{tr} \left(\tilde{\mathbf{C}}^{-1} \mathbf{P}^l \tilde{\mathbf{C}}^{-1} \mathbf{P}^{l'} \right) \quad (43)$$

where $\tilde{\mathbf{C}}^{-1} = \mathbf{S}^{-1/2} \tilde{\mathbf{A}}^{-1} \mathbf{S}^{1/2} \tilde{\mathbf{N}}^{-1}$. Since $\tilde{\mathbf{A}}^{-1}$ and $\tilde{\mathbf{N}}^{-1}$ have already been computed when forming the preconditioner, and since \mathbf{P}^l consists only of zeros and ones along the diagonal, calculating this approximate Fisher matrix only entails the multiplication of block diagonal matrices, which is relatively quick. It is important to note that the Newton-Raphson method only requires an approximate Fisher matrix to converge to the maximum likelihood solution – the final solution is independent of the Fisher matrix.

Of course any subsequent analysis of the power spectrum, such as cosmological parameter fitting, requires accurate error estimates for the c_l . These are often obtained by assuming the c_l are Gaussian distributed and computing their covariance matrix \mathbf{F}^{-1} . This description is likely to be fine for large l (say $l > 32$) but for small l we would like a better description. One could attempt to compute the distribution of the c_l directly from the Monte Carlo simulations, *independent* of any assumptions of Gaussianity. Specifically, for each realization i , we could estimate the maximum likelihood power spectrum $c_l^{(i)}$ using equation (15) which may be cast in the form

$$c_l^{(i)} = c_l^{ML} + \frac{1}{2} \tilde{\mathbf{F}}^{-1} (\mathbf{q}^{(i)} - \langle \mathbf{q} \rangle) \quad (44)$$

where c_l^{ML} is the maximum likelihood spectrum obtained from the data. Since all of these quantities have been precomputed, we can quickly obtain an estimate of the c_l distribution. However, it does assume that we obtain the maximum likelihood solution for each realization in a single iteration. Since we only have an approximate Fisher matrix to work with this is not strictly true – we should really iterate to convergence for each realization. Unfortunately, this implies a fresh computation of $\text{tr}(\mathbf{C}^{-1} \mathbf{P}^l)$ for each i , which is prohibitively costly. Since the assumption of Gaussianity only fails for low l , we recommend this procedure up to $l = 32$, for which it is computationally feasible.

For higher order multipoles, we need only compute the Fisher matrix. In principle we can use our Monte Carlo results to compute

$$\mathbf{F}_{ll'} = \frac{1}{2} \left\langle \mathbf{m}^T \mathbf{C}^{-1} \mathbf{P}^l \mathbf{C}^{-1} \mathbf{P}^{l'} \mathbf{C}^{-1} \mathbf{m} \right\rangle. \quad (45)$$

Unfortunately this is a factor of $N_{iter} l_{max}$ times more expensive than computing $\text{tr}(\mathbf{C}^{-1} \mathbf{P}^l)$, which is prohibitive. However, we have already noted that

$$\mathbf{F} = \frac{1}{4} \left\langle (\mathbf{q} - \langle \mathbf{q} \rangle) (\mathbf{q} - \langle \mathbf{q} \rangle)^T \right\rangle \quad (46)$$

Thus, in principle, one can obtain the Fisher matrix from the Monte Carlo simulations for free. In practice, we have found this to be a good recipe for computing the (comparatively large) diagonal elements, but to be too noisy for use in computing the (comparatively small) off-diagonal elements. To overcome this, we use the fact that the shape of the Fisher matrix (which also yields the window function for the c_l) depends mainly on the geometry of the weight map and only weakly on other aspects of the map. We therefore extract the shape of the approximate Fisher matrix $\tilde{\mathbf{F}}$ from equation (43) and renormalize to the variances obtained from the Monte Carlo simulations \mathbf{F}^{MC} i.e.

$$\mathbf{F}_{ll'} = \tilde{\mathbf{F}}_{ll'} \left(\frac{\mathbf{F}_{ll}^{\text{MC}} \mathbf{F}_{l'l'}^{\text{MC}}}{\tilde{\mathbf{F}}_{ll} \tilde{\mathbf{F}}_{l'l'}} \right)^{1/2} \quad (47)$$

Note that for large l , where the signal-to-noise becomes low due to beam smearing, the off-diagonal terms in the Fisher matrix start to become significant. This is easy to understand intuitively: the statistics of the c_l at large l are dominated by noise, which is not rotationally invariant (see Appendix A). This induces correlations amongst the multipoles. However, for the signal-to-noise ratio of the 2-year *MAP* data, this effect is unimportant (see Figure 3). We find that our results for χ^2 change by very little if we approximate the Fisher matrix as diagonal.

We emphasize that our *final* Fisher matrix is extremely accurate and may be used in good faith for parameter estimation. The calculation of the diagonal elements is exact and may be performed to arbitrary accuracy by increasing the number of Monte Carlo simulations. The scaling of the off-diagonal elements is approximate and uses the azimuthally averaged noise map. However, the off-diagonal elements make a small contribution to the Fisher matrix to begin with, as quantified by the small change in χ^2 . The effect of excluding non-azimuthal corrections, which are down by another two orders of magnitude (Figure 1), is therefore utterly negligible. Thus, while it is possible to make perturbative corrections to the scaling of the off-diagonal elements, this is unnecessary in practice. Another way of saying this is that the dominant source of cross talk among multipoles in the Fisher matrix is the galactic cut. Note that the neglect of azimuthal noise variations would *not* be valid for the diagonal elements since it would lead to an underestimate of the variance.

One should be careful in the choice of c_l used to compute the final Fisher matrix. It is *not* correct to use the recovered c_l because they are noisy. Any l for which we recovered a low c_l would be assigned a spuriously small error, and hence be given more weight in any subsequent analysis. This would consistently bias any fit to the power spectrum in the direction of less power. We therefore invoke our prior expectation that the underlying power spectrum is smooth, and smooth the recovered c_l with a spline prior to forming our final error estimates (see Appendix B for the smoothing procedure).

6. Estimating Cosmological Parameters

If we have a cosmological model that appears to be a good fit to the data, we can use the likelihood approach to directly compute cosmological parameters from a map. Rather than solve for the power spectrum c_l , we can solve for a set of parameters, $\mathbf{p} = (\Omega_b, \Omega_{CDM}, H_0, \text{etc.})$, that predict the spectrum.

Proceeding as in §2, we can maximize the likelihood function for \mathbf{p} by expanding it as a Taylor series around its maximum at $\bar{\mathbf{p}}$

$$f \equiv -2 \ln \mathcal{L} = \bar{f} + \sum_l \left. \frac{\partial f}{\partial p_k} \right|_{\bar{\mathbf{p}}} (p_k - \bar{p}_k) + \sum_{k,k'} \frac{1}{2} \left. \frac{\partial^2 f}{\partial p_k \partial p_{k'}} \right|_{\bar{\mathbf{p}}} (p_k - \bar{p}_k) (p_{k'} - \bar{p}_{k'}) \quad (48)$$

which leads to the analog of equation (15)

$$p_k^{(n+1)} = p_k^{(n)} - \frac{1}{2} \sum_{k'} \mathbf{F}_{kk'}^{-1} \left. \frac{\partial f}{\partial p_{k'}} \right|_{\mathbf{p}^{(n)}}. \quad (49)$$

The derivatives of the likelihood function may be computed using the chain rule

$$\left. \frac{\partial f}{\partial p_k} \right|_{\mathbf{p}} = \sum_l \left. \frac{\partial f}{\partial c_l} \right|_{c_l(\mathbf{p})} \left. \frac{\partial c_l}{\partial p_k} \right|_{\mathbf{p}}. \quad (50)$$

Similarly, the Fisher matrix of the parameters is given by

$$\begin{aligned} \mathbf{F}_{kk'} &= \left\langle - \left(\frac{\partial^2}{\partial p_k \partial p_{k'}} \right) \ln \mathcal{L} \right\rangle \\ &= \sum_{ll'} \frac{\partial c_l}{\partial p_k} \left\langle - \left(\frac{\partial^2}{\partial c_l \partial c_{l'}} \right) \ln \mathcal{L} \right\rangle \frac{\partial c_{l'}}{\partial p_{k'}} \\ &= \sum_{ll'} \frac{\partial c_l}{\partial p_k} \mathbf{F}_{ll'} \frac{\partial c_{l'}}{\partial p_{k'}}. \end{aligned} \quad (51)$$

The model power spectra may be computed with a fast numerical code (Seljak & Zaldarriaga 1996) and the partial derivatives $\partial c_l / \partial p_k$ may be computed using a finite difference approximation, typically using differences of order 2% of each parameter's value. As before, one computes the first and second derivatives of the likelihood function with respect to the c_l (equations (9) and (13)) via Monte Carlo techniques.

In practice, using Newton-Raphson as a root finding technique in parameter space is less straightforward than when solving for the power spectrum c_l . The radius of convergence, the region in which the Taylor expansion is valid, is substantially smaller. Its scale is set by $(\mathbf{F}^{-1})_{kk}^{1/2}$. In addition, the near degeneracies between various parameters create narrow

valleys in likelihood space for which a Newton approach is not optimal. Techniques exist which could overcome these difficulties, e.g. the Levenberg-Marquardt method (Press et al. 1992), which employs a control parameter λ to smoothly modulate between a steepest descent method ($\lambda \gg 1$) and a Newton method ($\lambda \ll 1$)

$$F_{l'} = F_{l'}(1 + \lambda \delta_{l'}). \quad (52)$$

Rather than developing such tools in this paper, we instead explore a simple χ^2 fit to the power spectrum

$$\chi^2(\mathbf{p}) = \sum_{l'} (c_l(\mathbf{p}) - c_l^{\text{recovered}}) \mathbf{F}_{l'} (c_{l'}(\mathbf{p}) - c_{l'}^{\text{recovered}}). \quad (53)$$

We find that this gives an excellent approximation to maximizing the full likelihood function from the map. To see why, consider the probability distribution of cosmological parameters given the recovered c_l

$$\mathcal{L}(\mathbf{p}|c_l) \propto \frac{1}{\det \mathbf{F}^{-1}} \exp \left[-\frac{1}{2} \delta \mathbf{c}(\mathbf{p})^T \mathbf{F} \delta \mathbf{c}(\mathbf{p}) \right]. \quad (54)$$

χ^2 fitting is a maximum likelihood estimator in the limit where \mathbf{F} is constant. Since \mathbf{F} has contributions from the assumed cosmological signal (which is being varied) as well as from pixel noise, this is not strictly the case. However, as we demonstrate below, we determine the power spectrum with excellent precision at low l . For $l > 600$, where the confidence bands begin to broaden, the signal to noise drops rapidly due to beam smearing. In this regime fixed pixel noise is the dominant contribution to the variance of the c_l . Overall, we have excellent knowledge of the Fisher matrix before we begin a χ^2 fit, so holding \mathbf{F} constant is an excellent approximation. A consistency check may be performed by comparing the power spectrum of the best fit cosmological model to the spline fit of the recovered power spectrum. If the two are very close, the Fisher matrices computed from either one will be virtually indistinguishable.

7. Results

In this section, we apply our numerical techniques to a realistic simulation of the *MAP* data. We simulate two years of W band (94 GHz) data using our current best estimate for the detector noise. We apply a Galactic plane cut that excludes the region $|b| < 10^\circ$, and we cut an additional 5% of the sky at random to simulate the effect of excising extragalactic point sources. We assume that the noise is azimuthally symmetric in ecliptic coordinates and that its variance changes by a factor of two between the ecliptic pole and ecliptic plane.

The maps are generated on a grid of galactic longitude and latitude points (l, b) which result in smaller map pixels near the galactic poles (see Appendix A). We scale the noise per pixel inversely with pixel area, in addition to the intrinsic coverage variations.

We have obtained results for a 1024 by 2048 pixel map with power up to $l_{max} = 1024$, using 10 Monte Carlo simulations to compute $\text{tr}(\mathbf{C}^{-1}\mathbf{P}^l)$ and \mathbf{F} . With 10 simulations, our expected errors are 5% larger than the minimum variance limit. The entire process converged in 5 iterations and took 10 hours of cpu time on an 8 processor SGI Origin 2000 computer. The recovered power spectrum is shown in Figure 4. Note that some negative c_l at high l are to be expected. They reflect the fact that the variance in those modes was less than that expected from the noise alone. One could adopt a prior distribution to prevent the c_l from going negative. However, this would complicate the error analysis as the probability distribution of the c_l would become skewed.

Since we know the true input power spectrum, we can quantify the goodness of our fit by computing

$$\chi^2 = \sum_{l,l'} \delta c_l \mathbf{F}_{ll'} \delta c_{l'} \quad (55)$$

where $\delta c_l \equiv c_l^{\text{recovered}} - c_l^{\text{true}}$, and \mathbf{F} is the Fisher matrix of the input spectrum c_l^{true} . We compute \mathbf{F} using equation (47), with 128 Monte Carlo simulations to compute \mathbf{F}_{ll} . We use a large number of Monte Carlo simulations to ensure that we are comparing our results to the true minimum variance Fisher matrix. With $N_{dof} \equiv l_{max} - 1 = 1023$, we obtain $\chi^2/N_{dof} = 1.08$, in accordance with our expectation that it lie within the range $(1 + 1/N_{mc})(1 \pm \sqrt{2/N_{dof}}) = 1.1 \pm 0.05$ (1σ). We find that 67% of the points lie within the 1σ error band, and 95% lie within the 2σ band. In Figures 5 and 6 we plot $\delta \equiv \delta c_l / \sigma_l$, where $\sigma_l^2 \equiv (\mathbf{F}^{-1})_{ll}$ is the variance of each c_l . The distribution of errors is evidently Gaussian and has a mean value $\langle \delta \rangle = 0.01$ and a standard deviation $\langle (\delta - \langle \delta \rangle)^2 \rangle = 1.04$, indicating that our results are both unbiased and minimum variance.

A visually more impressive way to display the power spectrum recovery is to fit a smoothing spline to the recovered points. The details of the spline fit are given in Appendix B and the results are shown in Figure 7. Note that exploiting the prior that c_l is a smooth function of l allows us to come spectacularly close to the form of the underlying power spectrum. As described in Appendix B, we generate confidence regions on the fit by fitting splines to 128 Monte Carlo simulations of c_l and sorting the fits at each l . The spline smoothing parameter has been chosen objectively using a process called cross-validation, which is a bootstrap technique (see Appendix B). If different criteria are used to compute the smoothing parameter, wiggles may appear in the fit (generally at high l), but it will generally stay within the depicted confidence bands.

To estimate cosmological parameters, \mathbf{p} , we can use the spline fit as our best guess power spectrum for computing the Fisher matrix \mathbf{F} . (Since the spline fit power spectrum and the input power spectrum are virtually identical, we have simply reused the Fisher matrix of the input spectrum we have already computed.) We then minimize

$$\chi^2 = \sum_{ll'} (c_l(\mathbf{p}) - c_l^{\text{recovered}}) \mathbf{F}_{ll'} (c_{l'}(\mathbf{p}) - c_{l'}^{\text{recovered}}) \quad (56)$$

where $c_l(\mathbf{p})$ is computed for a given parameter set \mathbf{p} using CMBFAST (Seljak & Zaldarriaga 1996). We consider 6 free parameters: Ω_b , Ω_{CDM} , h , τ , n , and the normalization, and we allow for a cosmological constant term, Ω_Λ , to enforce a flat universe: $\Omega_b + \Omega_{CDM} + \Omega_\Lambda \equiv 1$. We minimize χ^2 using an adaptive non-linear least-squares routine in the PORT optimization package (Gay 1990) after diagonalizing the Fisher matrix so that χ^2 may be written as a sum of squares. The input model used was standard Cold Dark Matter (sCDM) with parameter values 0.1, 0.9, 0.5, 0.0, 1.0, respectively. A starting guess was obtained by finding the best-fit model to the spline fit by eye (in fact, the true underlying model was unknown to one of us at the time). The minimization routine recovered parameter values 0.09, 0.76, 0.53, 0.13, and 1.02, respectively. The standard errors on these parameters, as given by the parameter Fisher matrix, are 7×10^{-3} , 0.1, 0.02, 0.2, and 0.015, respectively. The best fit cosmological model yields $\chi^2/N_{dof} = 1.078$ with respect to the data, to be compared to 1.082 for the input model with respect to the data, both within the 2σ range of expected variations for χ^2 . The input power spectrum and the best fit model are plotted in Figure 8; they are virtually indistinguishable.

Note that since the power spectrum of the best-fit model agrees closely with the spline fit, we are being self-consistent in holding \mathbf{F} constant. If this did not occur, a computation that allowed \mathbf{F} to vary might be called for. However, to the extent that the spline represents a non-parametric estimate of the underlying power spectrum, such lack of agreement might indicate deficiencies in the model, which may not have enough degrees of freedom. If one cannot obtain a reasonable value of χ^2 , even with additional model parameters, then it would be reasonable to rule out that class of cosmological models.

8. Summary

We have developed an unbiased, minimum variance estimator for the power spectrum of temperature fluctuations in CMB maps. We have used it to estimate the power spectrum up to $l = 1024$ from a 2 million pixel map that simulates single frequency *MAP* data (94 GHz) with realistic instrument noise and sky cuts. In contrast with existing algorithms, which require $O(N^3)$ operations, our algorithm is $O(N^2)$, and thus can be run overnight on

existing workstations, rather than running for months at national supercomputing facilities. We anticipate further improvements in performance with more aggressive optimization (and parallelization) of the code.

In addition, we have estimated cosmological parameters from the recovered c_l and find we can recover the input model with good precision. Thus, the pipeline from differential time-ordered data to cosmological parameters is now complete and well within present day computational capabilities.

Possibilities for future work include extensions to multi-frequency and polarization data, as well as the inclusion of Galactic foregrounds and systematic effects, such as striping, in our treatment of the data. The former only incur a linear increase of order a few in the operations count, while the latter can be accounted for by including them in the Monte Carlo simulations.

9. Acknowledgements

We have benefited from discussions with Chuck Bennett, Peter Kostelec, Robert Lupton, Bill Press, George Rybicki, Michael Strauss, Max Tegmark, Michael Vogeley, and Ned Wright. SPO, DNS, and GH are supported by NASA's *MAP* Project.

REFERENCES

- Barrett, R., et al. 1994, Templates for the Solution of Linear Systems: Building Blocks for Iterative Methods (SIAM: Philadelphia). Available at <http://www.netlib.org/templates/Templates.html>
- Bennett, C.L., Hinshaw, G., Jarosik, N., Mather, J.C., Meyer, S.S., Page, L., Skillman, D., Spergel, D.N., Wilkinson, D.T., & Wright, E.L. 1995, BAAS, 187, 7109
- Bersanelli, et al. 1996, *COBRAS/SAMBA*, ESA (Paris)
- Bond, J.R. 1995, Phys. Rev. Lett., 74, 4369
- Bond, J.R., Efstathiou, G., & Tegmark, M. 1997, MNRAS, 291, L33
- Bond, J.R., Jaffe, A.H., & Knox, L. 1998, Phys. Rev. D, 57, 2117
- Dilts, G.A. 1985, Journal of Computational Physics, 57, 439
- Driscoll, J.R., & Healy, D.M. 1994, Advances in Applied Mathematics, 15, 202
- Gay, D.M. 1990, Computing Science Report No. 153, AT&T Bell Laboratories
- Górski, K.M. 1994, ApJ, 430, L85
- Górski, K.M. 1998, private communication
- Górski, K.M., Hinshaw, G., Banday, A.J., Bennett, C.L., Wright, E.L., Kogut, A., Smoot, G.F., & Lubin, P. 1994, ApJ, 430, L89
- Górski, K.M., Banday, A.J., Bennett, C.L., Hinshaw, G., Kogut, A., Smoot, G.F., & Wright, E.L. 1996, ApJ, 464, L11
- Hinshaw, G., Bennett, C.L., & Kogut, A. 1995, ApJ, 441, L1
- Hinshaw, G., Banday, A.J., Bennett, C.L., Górski, K.M., Kogut, A., Smoot, G.F., & Wright, E.L. 1996, ApJ, 464, L17
- Healy, D.M., Rockmore, D., Moore, S.S.B. 1996, Dartmouth College Technical Report PCS-TR96-292
- Jungman, G., Kamionkowski, M., Kosowsky, A., & Spergel, D.N. 1996, Phys. Rev. D, 54, 1332
- Knox, L. 1995, Phys. Rev. D, 52, 4307
- Kostelec, P. 1998, private communication
- Muciaccia, P.F., Natoli, P., & Vittorio, N. 1998, ApJ, 488, L63
- Press, W.H., Teukolsky, S.A., Vetterling, W.T., & Flannery, B.P. 1992, Numerical Recipes: The Art of Scientific Computing, 2nd Ed., (Cambridge: Cambridge University Press)

- Schulten, Klaus, & Gordon 1976, *Computer Phys.Comm.*, 11, 269. Code is available at <http://www.netlib.org/slatec/src/drc3jj.f>
- Seljak, U., & Zaldarriaga, M. 1996, *ApJ*, 469, 437
- Spergel, D.N. 1994, Warner Prize Lecture, *BAAS*, 185.7301
- Stroud, A.H. 1971, *Approximate Calculation of Multiple Integrals*, (Englewood Cliffs: Prentice-Hall)
- Taylor, M. 1995, *SIAM, J.Numer.Anal.*, 32, 667
- Tegmark, M. 1996, *MNRAS*, 288, 299
- Tegmark, M. 1997, *Phys. Rev. D*, 55, 5895
- Tegmark, M. & Bunn, E.F. 1995, *ApJ*, 455, 1
- Wahba, G. 1990, *Spline Models for Observational Data*, (SIAM, Philadelphia)
- Wright, E.L., Hinshaw, G., & Bennett, C.L. 1996, *ApJ*, 458, L53
- Zaldarriaga, M., Spergel, D.N., & Seljak, U. 1997, *ApJ*, 488, 1

A. Fast Spherical Harmonic Transforms

The algorithm presented in this paper relies heavily on the fact that we have available fast, $O(N^{3/2})$, forward and inverse spherical harmonic transforms on the sphere, as opposed to standard $O(N^2)$ transforms. We use a formulation which employs FFTs in ϕ , and thus requires that the map pixels be distributed on rows of constant θ . The scheme was first brought to the attention of the CMB community by Muciaccia, Natoli & Vittorio (1998). Alternative formulations exist (Dilts 1985) which also use FFTs in the θ direction. The most sophisticated implementation requires only $O(N(\log N)^2)$ operations for both transforms, by using fast Legendre transforms (Driscoll & Healey 1994, Healy, Rockmore & Moore, 1996). In practice, due to cache problems in the use of precomputed data, current implementations run no faster than the naive $O(N^{3/2})$ algorithms, though work is presently underway to remove this barrier (Kostelec 1998). For completeness, we summarize the transform method below.

Making maps – Given a set of a_{lm} ’s, we wish to evaluate

$$\delta t(\theta_i, \phi_j) = \sum_{l=0}^{l_{max}} \sum_{m=-l}^l a_{lm} Y_{lm}(\theta_i, \phi_j). \quad (\text{A1})$$

Now, observing that we can interchange the order of summation

$$\sum_{l=0}^{l_{max}} \sum_{m=-l}^l \longleftrightarrow \sum_{m=-l_{max}}^{l_{max}} \sum_{l=|m|}^{l_{max}} \quad (\text{A2})$$

we can write

$$\delta t(\theta_i, \phi_j) = \sum_{m=-l_{max}}^{l_{max}} e^{im\phi_j} q_m(\theta_i) \quad (\text{A3})$$

where

$$q_m(\theta_i) = \sum_{l=|m|}^{l_{max}} a_{lm} \sqrt{\frac{2l+1}{4\pi} \frac{(l-m)!}{(l+m)!}} P_m^l(\cos \theta_i). \quad (\text{A4})$$

The Legendre functions P_m^l may be generated using standard recursion relations. The obvious motivation for writing the expansion in this form is to employ FFT techniques in the evaluation.

What is our total operations count? At fixed θ_i , we need to generate l_{max}^2 q_m 's. (Note therefore that our memory storage requirements are $O(N)$, which is entirely feasible). Since there are n_θ θ_i 's to step through, the total operations count is $l_{max}^2 n_\theta \sim N^{3/2}$. The cost of the FFT at fixed ϕ_j is only $O(n_\phi \log n_\phi)$. Since there are n_ϕ ϕ_j 's to step through, the FFT's only cost $O(N \log N)$. Thus, to leading order, map making is an $O(N^{3/2})$ process.

Inverting maps – The formal inverse transform is defined in terms of an integral

$$a_{lm} = \int Y_{lm}(\Omega) \delta t(\Omega) d\Omega \quad (\text{A5})$$

which may be evaluated with a cubature formula

$$a_{lm} = \sum_i Y_{lm}(\Omega_i) \delta t(\Omega_i) w(\Omega_i) \quad (\text{A6})$$

where the integration weight $w(\Omega_i)$ is essentially the solid angle of pixel i . Assuming that our pixels are equally spaced in ϕ at a given θ , this may be cast in the form

$$q_m(\theta_i) = \sum_j e^{-im\phi_j} \delta t(\theta_i, \phi_j) \quad (\text{A7})$$

with

$$a_{lm} = \sum_i w(\theta_i) q_m(\theta_i) \sqrt{\frac{2l+1}{4\pi} \frac{(l-m)!}{(l+m)!}} P_m^l(\cos \theta_i) \quad (\text{A8})$$

where $w(\theta_i)$ is proportional to the pixel solid angle at θ_i .

In practice, we actually wish to evaluate expressions of the form

$$\tilde{a}_{lm} = \sum_i Y_{lm}(\Omega_i) f(\Omega_i) \quad (\text{A9})$$

where $f(\Omega)$ is some function on the sphere. These terms arise in the normal equations, (27) and (28), where f is an inverse variance weighted temperature map, and in the factorization of matrices into convolutions of a diagonal matrix with the spherical harmonics, as in equation (6). This expression is distinct from the formal inverse transform, but may be evaluated using the same FFT methods by substituting f for δt and omitting the integration weights.

The reader can easily verify that inverting maps is also an $O(N^{3/2})$ process requiring only $O(N)$ memory storage. One can also exploit various symmetries, such as $q_{-m} = q_m^*$, and $P_m^l(\cos(\pi - \theta)) = (-1)^{l+m} P_m^l(\cos \theta)$ to further speed up the transforms. In practice, we find the lion's share of cpu time for both the forward and inverse transforms is spent in generating the P_m^l . Since we already demand $O(N^{3/2})$ storage for the preconditioner matrix, it is only a modest increase to store the P_m^l in memory, which is also an $O(N^{3/2})$ requirement. (Note that only one hemisphere need be stored.) This generally leads to an order of magnitude decrease in cpu time: for example, the time required for each $l = 512$ transform is reduced from 25 s to 3 s. At present, we find that each $l = 1024$ transform takes about 25s as a single processor job on an SGI Origin 2000.

We close this Appendix with some comments about the role of pixels in the evaluation of inverse spherical harmonic transforms. The cubature formula provides a formal check on pixelization schemes by ensuring that pixelization errors are negligible, i.e. that there is no information loss in going from a continuous to a discrete field. Formally this implies specifying a grid Ω_i and integration weights $w(\Omega_i)$ such that the integration error

$$\epsilon = \sum_{i=1}^N w(\Omega_i) f(\Omega_i) - \int f(\Omega) d\Omega \quad (\text{A10})$$

vanishes when f is a polynomial of degree D . In this paper we employ a spherical product Gauss cubature formula for integrating over the sphere (see, e.g., Stroud 1971). This scheme has the property of requiring the minimum number of pixels for a given polynomial degree of any pixelization scheme. The grid points in ϕ are given by the zeroes of the Fourier basis sines and cosines (simply the equiangular grid), while the grid points in θ are given by the zeroes of the Legendre polynomial basis. Standard routines for calculating the grid points and weights, $w(\theta_i)$, for the associated Legendre quadrature formula exist (Press et al., 1992). This grid has negligible integration error and also has the slight advantage over a purely equiangular grid that the grid points and weights are a function of the

integration range. The arrangement of sampled points can therefore be made optimal for a sphere with a Galaxy cut. This pixelization scheme does have elongated pixels of smaller area near the poles. Thus, since pixel noise scales with pixel area, our scheme contains a disproportionately large number of noisy pixels near the poles. In practice, we have not found such endpoint apodizing to be harmful.

What are the optimal choices for n_θ and n_ϕ in terms of l_{max} ? In terms of the Gaussian cubature formula, the optimal choice is $n_\theta = l_{max} + 1$, $n_\phi = 2l_{max} + 1$, which integrates *exactly* the first $(l_{max} + 1)^2$ spherical harmonics. The accuracy of this grid is easily verified numerically by observing the exact orthonormality of the first $(l_{max} + 1)^2$ spherical harmonics on the full sky. (Note that *COBE* type pixelization schemes, which have equal area per pixel, require a substantially larger number of points to achieve the same accuracy.) Note that because the number of a_{lm} 's is half the number of integration points, the spherical harmonic transform is *not* invertible unless the integrated function is bandwidth limited to $l_{max} + 1$. Indeed, it has been proven (Taylor 1995) that there does not exist *any* cubature-based discrete spherical harmonic transform with the same number of points as spectral coefficients. An intuitive way to understand this is to note that the spherical harmonics span a subspace of S^2 which is invariant under rotations of the sphere. Thus, for a function that respects such symmetries and thus can be expanded in spherical harmonics, much of the information content in the sampled points is redundant and is annihilated in the spherical harmonic basis.

For practical purposes, the CMB signal is band-width limited, as beam smearing virtually destroys any signal above some l_{max} . However, the noise map is not bandwidth limited and cannot be projected onto a finite set of spherical harmonics. We see that by noting that the underlying weight map is not rotationally invariant, in general, which is why the noise matrix $\mathbf{N}_{(lm)(lm)'}$ is dense, even over the full sky. This has important practical consequences when maximizing the likelihood function. In particular, one is not free to transform between pixel and spherical harmonic space. It is impossible, for instance, to precondition in spherical harmonic space and maximize the likelihood in pixel space: the (essentially noise) eigenvalues are wiped out in spherical harmonic space but are retained in pixel space.

We emphasize that our algorithm is independent of the pixelization scheme, as long as fast spherical harmonic transforms are available. For instance, the HEALPIX scheme (Gorski 1998), which uses equal area pixels, is also a viable option.

B. Spline Fitting

We have presented an algorithm for extracting the minimum variance power spectrum, c_l , and its error matrix, \mathbf{F}^{-1} , from a map. This is all that is needed to make comparisons with Gaussian theoretical models. However, there are at least two good reasons why one would like to fit a smooth curve to the c_l data. 1) We have argued that it is better to construct the experimental Fisher matrix from the smoothed c_l to avoid bias in any subsequent analysis. 2) For the purpose of visual presentation we would like an aid to guide the eye through a forest of data points.

The usual smoothing procedure is to either bin the data or employ a moving average, which reduces the errors by \sqrt{n} , where n is the number of points in each bin. The drawback of such a procedure is that while the zeroth- and first-order moments of the data are preserved, higher order moments are not. In particular, if the underlying function has a non-zero second derivative (e.g., at an acoustic peak), a bias is introduced (Press et al. 1992). A significant improvement would be to approximate the data as piecewise polynomial, rather than piecewise constant, as with Savitzky-Golay smoothing filters (Press et al. 1992).

However, we advocate fitting a least-squares weighted smoothing spline (Wahba 1990) to the recovered c_l . Such a fit is non-parametric and model-independent in the sense that we allow ourselves $l_{max} - 1$ degrees of freedom. We find the cubic spline $f(l)$ which minimizes the quantity

$$\sum_{l'} (f(l) - c_l) \mathbf{F}_{ll'} (f(l') - c_{l'}) + \lambda \int f''(l) dl. \quad (\text{B1})$$

The smoothing parameter λ , which controls the usual trade-off between smoothness and fidelity to the data, is chosen to satisfy the relation

$$(l_{max} - 1) - \sqrt{2(l_{max} - 1)} < \chi^2 < (l_{max} - 1) + \sqrt{2(l_{max} - 1)} \quad (\text{B2})$$

where $\chi^2 \equiv \sum_{ll'} (f(l) - c_l) \mathbf{F}_{ll'} (f(l') - c_{l'})$. The slight freedom we have in selecting λ within this range is analogous to the freedom we have to select a bin size in an averaging scheme. We proceed with the fit iteratively: first, employing the Fisher matrix of the unsmoothed data, we construct a preliminary smoothing spline. Next, generating a new Fisher matrix from $f(l)$, we construct a second and final smoothing spline.

An alternative approach to choosing λ is to use cross-validation. This is essentially a bootstrap technique in which λ is chosen so that the spline best approximates the data at any given l if it is computed with all the data except c_l . In general, the two methods give similar results. The fits in this paper were obtained using cross-validation.

To compute errors on our spline fit, we employ bootstrap resampling. Specifically, we calculate the exact Fisher matrix from $f(l)$ and generate a series of synthetic power spectra, $c_l^{(i)}$ from this Fisher matrix. This will be accurate to the extent that we have accurately computed \mathbf{F} . One can also generate $c_l^{(i)}$ assuming they are drawn from distributions with dispersion $(\mathbf{F}^{-1})_{ll}^{1/2}$, which ignores correlations between the c_l . The two methods give very similar results. We then compute the smoothing spline for each realization $c_l^{(i)}$ and sort the results at each l . This allows us to generate confidence intervals for the spline fits. Figure 7 shows the customary 68% confidence band.

The use of a smoothing spline entails a small but non-negligible bias because the mean of the Monte Carlo spline fits does not equal the input power spectrum. Such effects are well-known (Wahba 1990). We calibrate this bias from the Monte Carlo simulations and apply it to our best fit spline and confidence bands. Note also that the confidence bands of the spline fit are not symmetric about the mean value, particularly near a peak. The use of Monte Carlo simulations gives us the probability distribution of the spline fits and thus a firm handle on such effects.

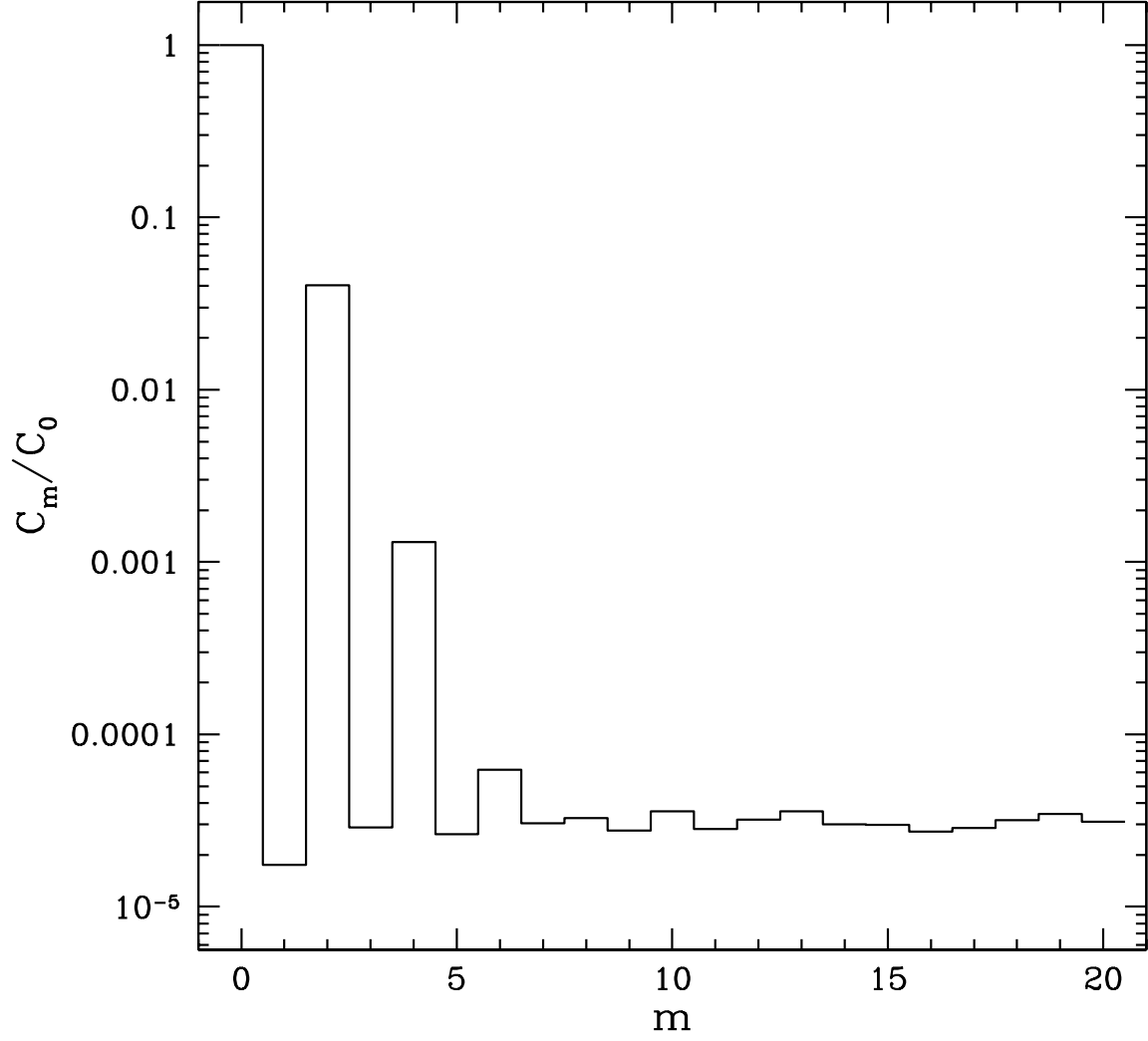


Fig. 1.— Normalized c_m vs m , where $c_m \equiv \sum_{l=m}^{l_{max}} |\mathbf{w}_{lm}|^2 / (l_{max} + 1 - m)$ and \mathbf{w}_{lm} is the spherical harmonic expansion of the weight map $1/\sigma_i^2$. Note that only the $m = 0, 2, 4, 6$ terms are significant, implying that \mathbf{N}^{-1} is in fact very sparse. The baseline extending out to high m is contributed by the pixels cut due to point sources; it disappears if there are no such cuts.

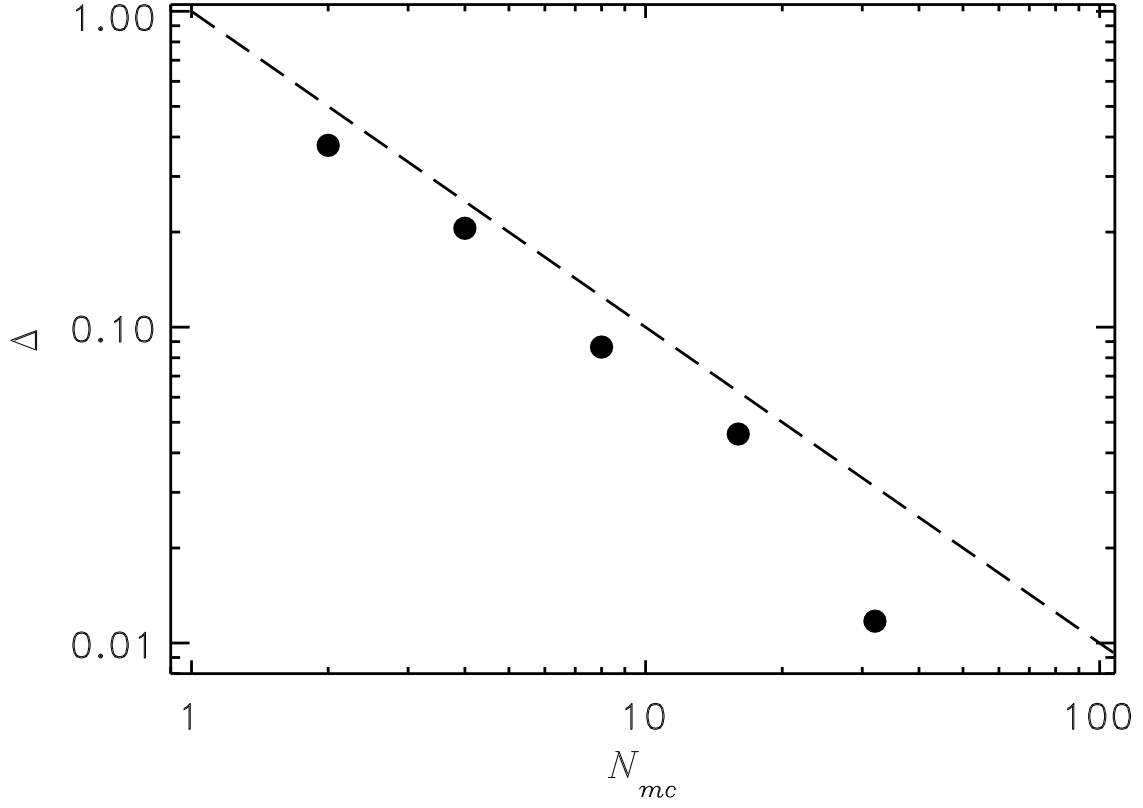


Fig. 2.— Plot of $\Delta \equiv \chi^2/(l_{max} - 1) - 1$ vs. number of Monte Carlo simulations used to compute $\text{tr}(\mathbf{C}^{-1}\mathbf{P}^l)$. This result is based on solving for c_l from a given 512×1024 pixel map. Our expectation that $\Delta \propto 1/N_{mc}$ (dashed line) is met.

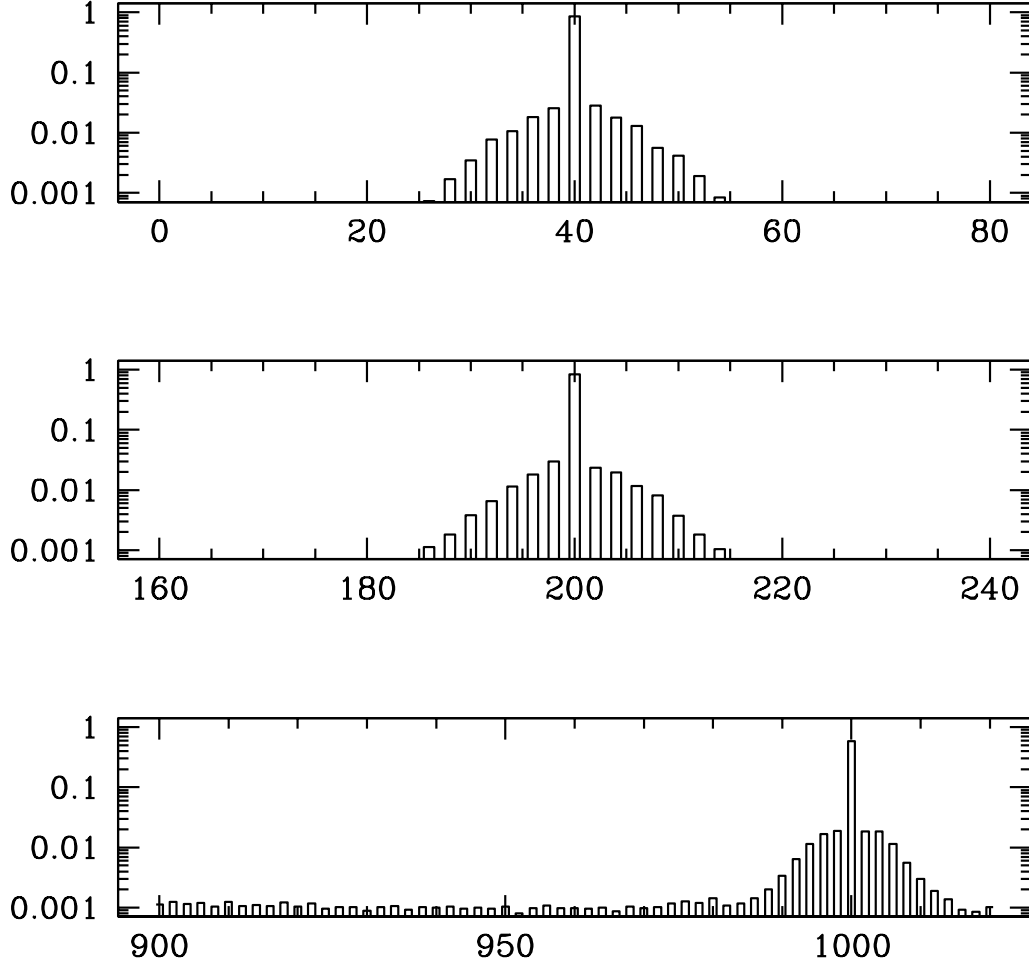


Fig. 3.— Window functions at various l . At high signal to noise, we observe the well-known translational independence of the window function. The small size of the galactic cut allows for an extremely narrow window function. At low signal to noise correlations between widely separated l appear, but remain very weak.

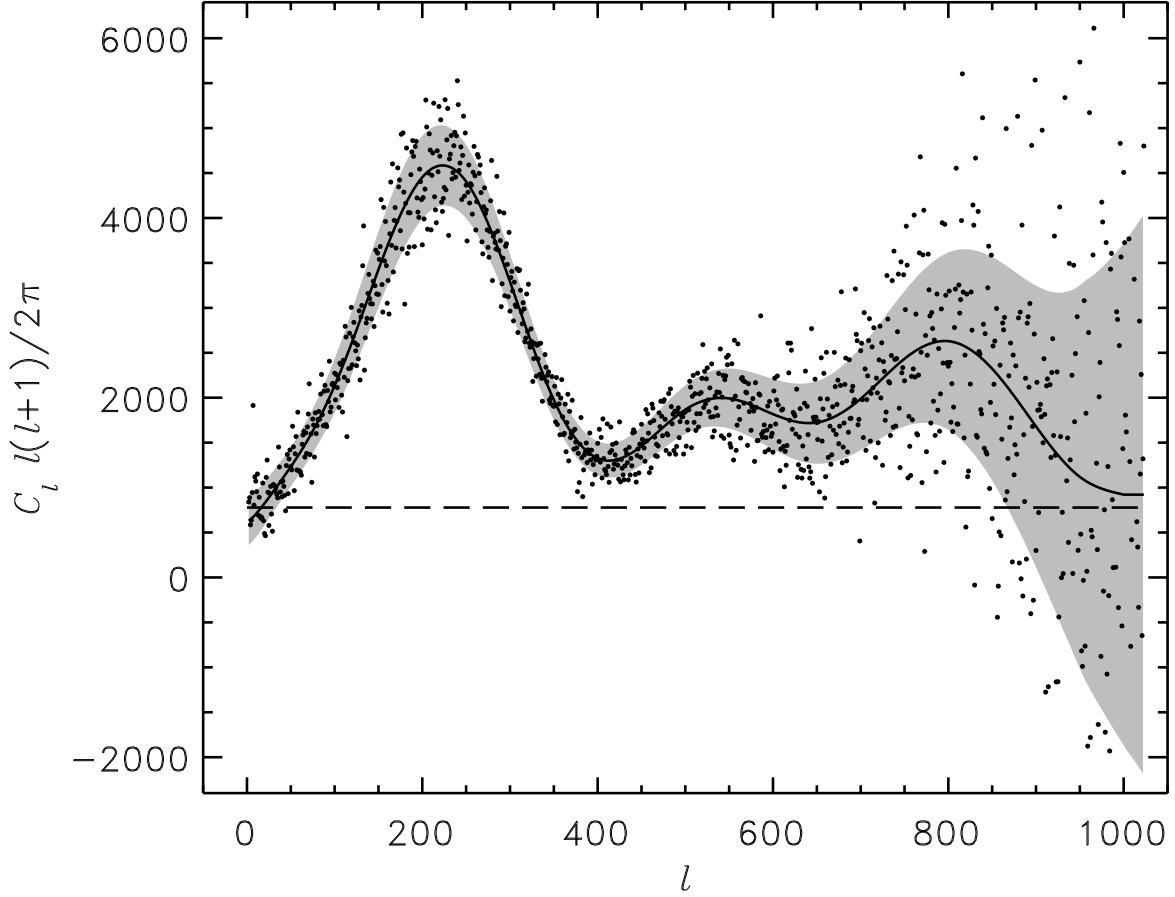


Fig. 4.— Recovered power spectrum c_l for a single simulated 1024×2048 pixel map. 10 Monte Carlo simulations were used to compute $\text{tr}(\mathbf{C}^{-1}\mathbf{P}^l)$. The grey band indicates the one sigma uncertainty given by $(\mathbf{F}_l^{-1})^{1/2}$. The light dashed line indicates the starting guess. This run converged in 3 iterations using the approximate method and 2 subsequent iterations using the Monte Carlo method and took approximately 10 hours as an 8 processor job on an SGI Origin 2000 computer. See Figure 7 for an indication of how well the power spectrum can be recovered under the assumption that it is a smooth function of l .

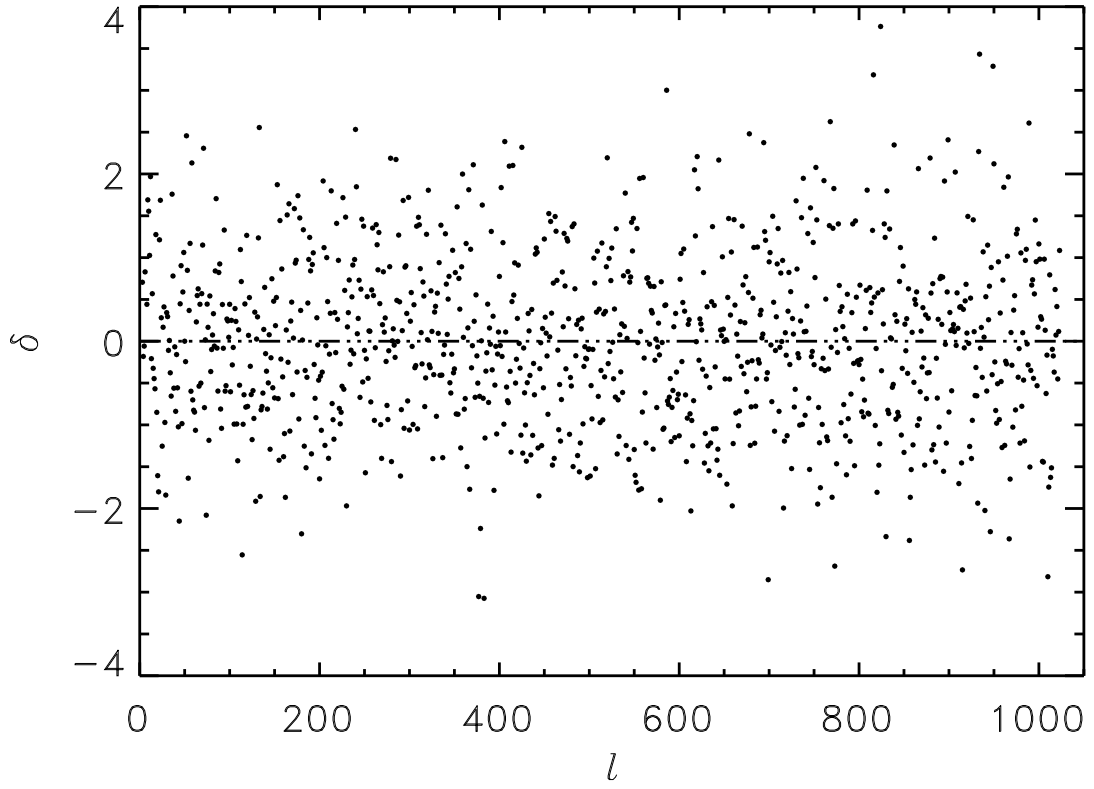


Fig. 5.— Scatter plot of $\delta \equiv (c_l^{\text{recovered}} - c_l^{\text{true}})/\sigma_l$, where c_l^{true} is the input power spectrum, $c_l^{\text{recovered}}$ is the recovered spectrum shown in Figure 4, and $\sigma_l \equiv (\mathbf{F}^{-1})_{ll}^{1/2}$.

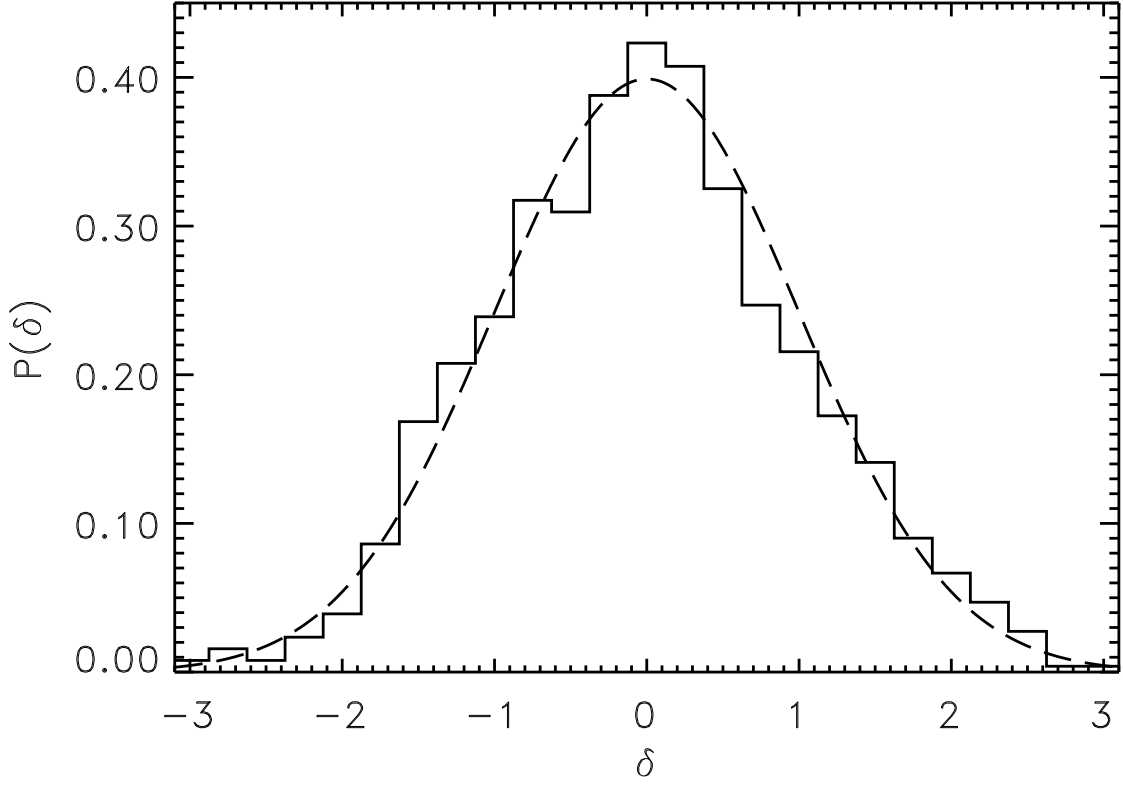


Fig. 6.— Histogram plot of the distribution of $\delta \equiv (c_l^{\text{recovered}} - c_l^{\text{true}})/\sigma_l$. Also depicted is a Gaussian distribution of zero mean and unit variance; the two distributions agree closely. 67% of the points lie between $\delta = -1$ and $\delta = +1$, and 95% of the points lie between $\delta = -2$ and $\delta = +2$.

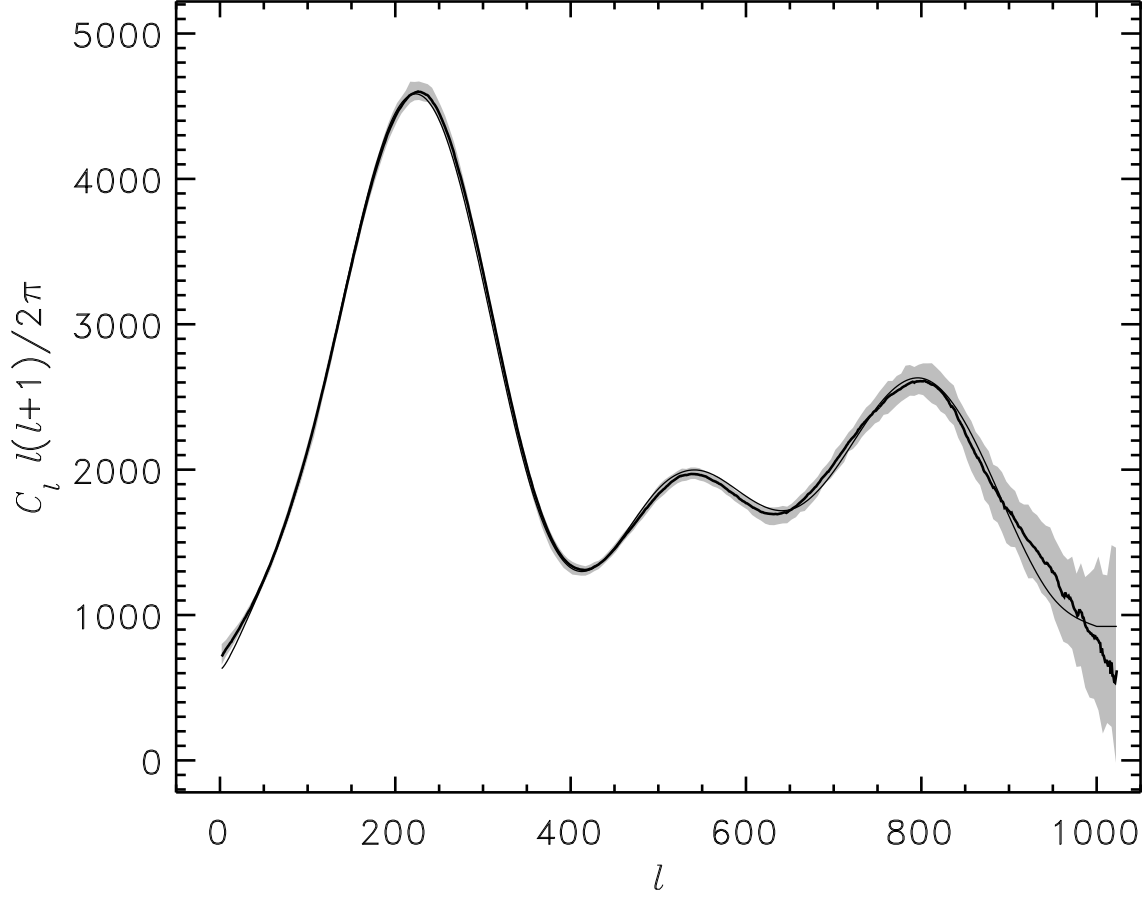


Fig. 7.— The result of a smoothing spline fit to the points in Figure 4. The dark solid line is the spline fit, the light solid line is the input power spectrum. The grey band indicates the 68% confidence band obtained from bootstrap simulations. Including the prior expectation that the underlying power spectrum is smooth allows one to obtain a very firm handle on the power spectrum.

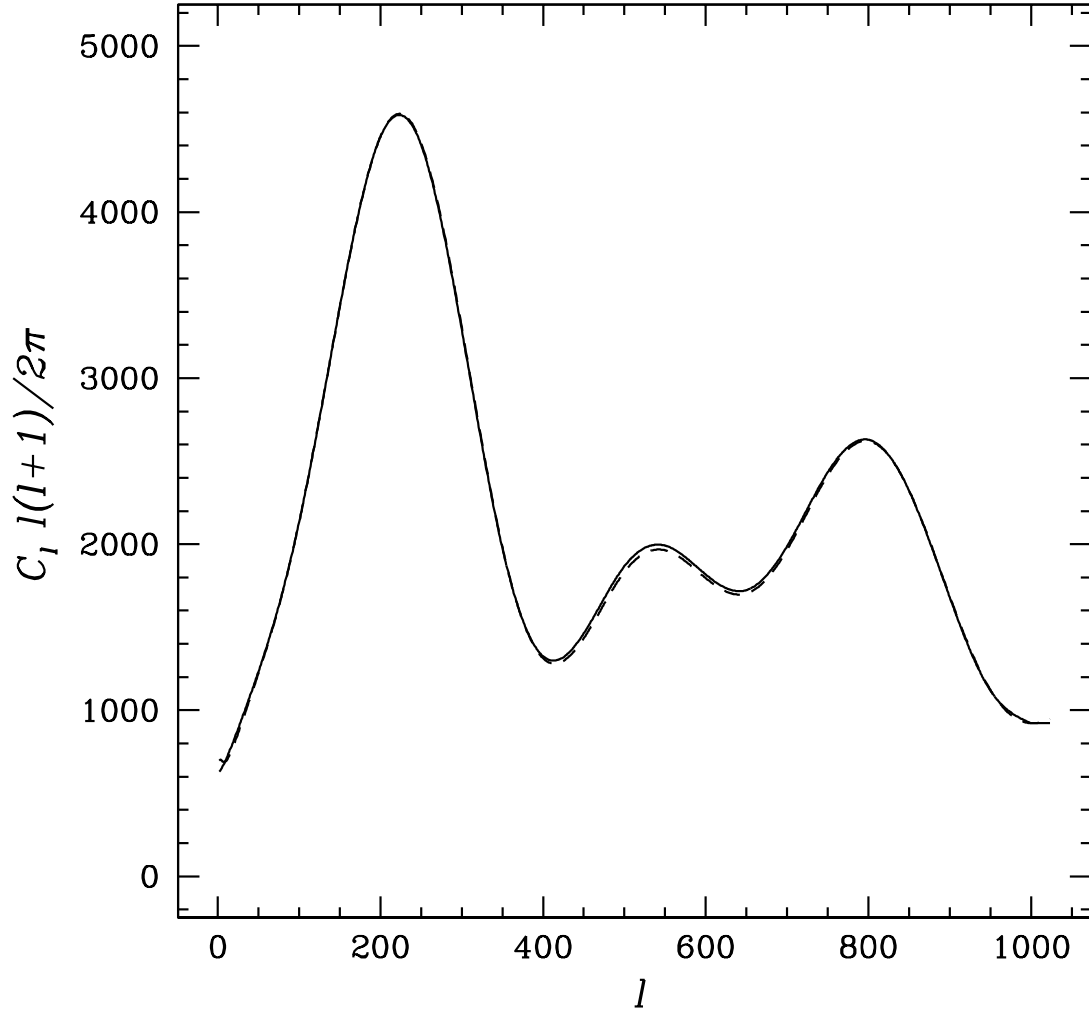


Fig. 8.— The solid line indicates the input power spectrum, while the dashed line indicates the best-fit cosmological model from the data. The two are virtually identical.